Simultaneous transfer ionization in a positron-helium atom system

B. Nath[1,2] and C. Sinha[1]
[1]*Department of Theoretical Physics, Indian Association for the Cultivation of Science, Jadavpur, Calcutta 700032, India*
[2]*Kumar Ashutosh Boys Institution (Main) 10/1, Dum Dum Road, Calcutta 700030, India*
(Received 14 June 1999; revised manuscript received 9 December 1999; published 10 May 2000)

The simultaneous electron capture and the ejection of another electron by which a doubly charged He ion and a Ps atom are produced in a single collision between a positron and a He atom is investigated theoretically. The angular distributions of the Ps atom as well as of the ejected electron are studied in the low-and intermediate-(100–500 eV) energy regime with respect to the threshold energy for the transfer ionization process. The electron-electron correlation effect which mainly governs such two-electron transition processes has been taken into account in both the initial and final channels. The fully differential cross sections for different dynamics reveal some structures which are to be verified by the future experiments.

PACS number(s): 34.70.+e, 34.90.+q

I. INTRODUCTION

Recently, studies on the electron-electron correlation effect in different collisional processes are finding increasing attention from both theoretical and experimental physicists. Particularly the two-electron transition processes, e.g., double ionization (DI), double capture (DC), simultaneous excitation ionization (EI), transfer ionization (TI), etc., in multielectron atoms are mainly governed by the electron-electron correlation effect. The role of electron correlation in the context of different atomic collisions has been emphasized by several authors [1–6]. Various theoretical models have been proposed to account for the electron-electron correlation effect (arising due to Coulomb interactions) in different ways for studying the above-mentioned two-electron transition processes.

In the present work we study the simultaneous capture (transfer) and ionization of the two target electrons of a helium atom, commonly known as transfer ionization (TI) in which the incident positron (e^+) captures an electron from the He atom while the other electron gets ionized simultaneously, i.e.,

$$e^+ + \mathrm{He} \rightarrow (e^+ e) + e + \mathrm{He}^{++}. \tag{1}$$

For heavy-particle impact, e.g., in a proton-helium collision, a number of differential measurements (angular distributions) [7–9] have been performed on the simultaneous transfer and ionization (TI) of the two bound electrons resulting in the production of a fully stripped He^{++} ion. However, for a light projectile, the first differential measurement was reported [10] for the TI process in a positron-argon atom collision, where one of the electrons from the outermost shell of the argon atom is captured by the incident positron to form a positronium atom (Ps) while another electron gets ionized in a single collision. This measurement has stimulated us for the present theoretical study. Later, some other measurements [11,12] have been reported for the double ionization (DI) of some noble gases by e^+ impact where both the direct ionization as well as ionization with Ps formation (i.e., TI) cross sections have been measured. The latter experiments [11,12] refer to the measurements of the total cross sections only. However, though the experimental data exist mainly for some complex noble-gas atoms, we have chosen for our first work, the helium atom to be the target, since the latter is the simplest system to be studied for two-electron transition processes. From the experimental point of view, it is much easier to measure the data of total cross sections (for the process concerned) than for the differential ones, while the reverse is true from the theoretical point of view. In the present work we have studied the fully differential cross sections for the simultaneous TI process in a positron-helium atom system. As a first step we have considered the case when the Ps atom is formed in the ground state only although there is a probability that the Ps may be formed in excited state as well [10]. To our knowledge, the present work is the first theoretical attempt for such a TI process by positron impact. Theoretically, the transfer-ionization process can occur mainly through the following two possible mechanisms. In one case the positron can interact with one of the electrons of a He atom to form a Ps atom while the other electron is ejected due to the electron-electron correlation effect. Another possibility is that the positron interacts with both the electrons independently by turn, causing the formation of the Ps atom as well as the ejection of an electron. The latter process is a second-order process since it involves two successive binary collisions and should be treated in the framework of a second-order theory (e.g., second Born). The present prescription has been formulated on the basis of the first mechanism.

II. THEORY

The prior form of the transition-matrix element for the TI process (1) is given by

$$T_{if} = \langle \Psi_f^-(\mathbf{r}_1, \mathbf{r}_2, \mathbf{r}_3) | V_i | \psi_i(\mathbf{r}_1, \mathrm{r}_2, \mathbf{r}_3) \rangle. \tag{2}$$

The total Hamiltonian H of the system is written as

$$H = H_0 + \frac{Z_t}{r_1} - \frac{Z_t}{r_2} - \frac{Z_t}{r_3} - \frac{1}{r_{12}} - \frac{1}{r_{13}} + \frac{1}{r_{23}}, \tag{3}$$

where $Z_t = 2$ is the charge of the target He atom.

The full kinetic energy operator is given by

$$H_0 = -\frac{1}{2}\nabla_1^2 - \frac{1}{2}\nabla_2^2 - \frac{1}{2}\nabla_3^2, \tag{4}$$

where $\mathbf{r}_1$, $\mathbf{r}_2$, and $\mathbf{r}_3$ are the position vectors of the incoming electron and the two bound electrons ''2'' and ''3,'' respectively, with respect to the target nucleus; $\mathbf{r}_{12}=\mathbf{r}_1-\mathbf{r}_2$; $\mathbf{r}_{23}=\mathbf{r}_2-\mathbf{r}_3$; $\mathbf{r}_{13}=\mathbf{r}_1-\mathbf{r}_3$. The initial channel wave function ψ_i in Eq. (2) is chosen as

$$\psi_i(\mathbf{r}_1,\mathbf{r}_2,\mathbf{r}_3) = \exp(i\mathbf{k}_i\cdot\mathbf{r}_1)\varphi_i(\mathbf{r}_2,\mathbf{r}_3), \tag{5}$$

where $\mathbf{k}_i$ is the initial momentum of the incident particle and $\varphi_i(\mathbf{r}_2,\mathbf{r}_3)$ is the correlated wave function [13] of the ground-state helium atom given by

$$\varphi_i(\mathbf{r}_2,\mathbf{r}_3) = N_i[\exp(-\lambda_a r_2-\lambda_b r_3)+\exp(-\lambda_b r_2-\lambda_a r_3)] \times[1+C_0\exp(-\lambda_c r_{23})] \tag{6}$$

with $N_i=1.6383$, $\lambda_a=1.4096$, $\lambda_b=2.2058$, $\lambda_c=0.242$, and $C_0=-0.6054$.

In view of Eqs. (2)–(5), the perturbation interaction V_i [in Eq. (2)] in the initial channel is obtained as

$$V_i = \frac{Z_t}{r_1} - \frac{1}{r_{12}} - \frac{1}{r_{13}}. \tag{7}$$

Equation (7) shows that the perturbation V_i vanishes asymptotically (for $r_1\to\infty$ and r_2, r_3 finite).

In the present model, the projectile is assumed to interact only with one of the bound electrons to be transferred while the ejection of the other electron is supposed to be caused by the electron-electron correlation effect. The final-state wave function Ψ_f^- in the present prescription is chosen as

$$\Psi_f^-(\mathbf{r}_1,\mathbf{r}_2,\mathbf{r}_3) = \exp(i\mathbf{k}_f\cdot\mathbf{R})\exp(-\lambda_f|\mathbf{r}_1-\mathbf{r}_2|)M_3\exp(i\mathbf{k}_3\cdot\mathbf{r}_3)\ {}_1F_1(i\alpha_3,1;-i(k_3r_3+\mathbf{k}_3\cdot\mathbf{r}_3)) \times(2\pi)^{-3/2}M_2\ {}_1F_1(i\alpha_2,1;-i(k_2r_2+\mathbf{k}_2\cdot\mathbf{r}_2))M_{23}\ {}_1F_1(i\alpha_{23},1;-i(k_{23}r_{23}+\mathbf{k}_{23}\cdot\mathbf{r}_{23})), \tag{8}$$

where $\alpha_2=-(Z-1)/k_2$, $\alpha_3=-Z/k_3$, $\alpha_{23}=1/2k_{23}$, $|\mathbf{k}_2|=|k_f/2|$, $\mathbf{k}_{23}=(\mathbf{k}_2-\mathbf{k}_3)/2$, $\mathbf{R}=(\mathbf{r}_1+\mathbf{r}_2)/2$, and $M_j=\exp(\pi\alpha_j/2)\Gamma(1-i\alpha_j)$ with $j=2$, 3, or 23; λ_f is the bound-state parameter for the ground-state Ps atom and is given by $\lambda_f=0.5$.

The construction of the present final-state wave function takes account of the fact that the ejected electron (r_2) first attains a continuum state of its parent nucleus (He^+ ion) and then by virtue of the $1/r_{12}$ interaction, is finally captured by the incident positron to form the positronium atom (Ps) in its ground state. In the present prescription, the electron-electron correlation effect which mainly governs the simultaneous two-electron transition, has been taken into account in both the initial and the final channels. The Ps atom could also be formed in the excited state (e.g., $2s$,$2p$) though the probability of such a process is expected to be much lower. However, the present work concentrates only on the formation of a ground state Ps atom.

The excess energy ($E_i-E_{\rm th}$) in this transfer-ionization process is shared by the two outgoing particles, e^- and Ps. In the TI process the energy and momentum exchange occurs between the projectile, the electron to be captured, as well as the other bound electron that is ionized. Thus the energy conservation relation for the process concerned is given by

$$k_i^2/2 + \in_{\rm He} = k_f^2/2\mu_f + k_3^2/2 + \in_{\rm Ps}, \tag{9}$$

where μ_f is the reduced mass in the final channel. $\mathbf{k}_i$, $\mathbf{k}_3$, and $\mathbf{k}_f$ are the respective wave vectors of the incident positron, ejected electron, and the scattered Ps atom; $\in_{\rm He}$ and $\in_{\rm Ps}$ are the binding energies of the ground-state helium atom and the Ps atom, respectively. The transition amplitude is finally reduced [14,15] to a three-dimensional integral which has been evaluated numerically. The fully (triple) differential cross section (TDCS) for this TI process is given by

$$d^3\sigma/dE_2 d\Omega_1 d\Omega_2 = \frac{k_f k_3}{\mu_f k_i}|T_{if}|^2. \tag{10}$$

In order to have an idea about the importance of the final channel correlation as well as some other higher-order effects, we have also calculated the first-Born cross sections for the present TI process in which the correlation effect in the final channel is neglected while the same initial channel correlation is retained. The corresponding expression of the amplitude is given by

$$T_{if}^B = \left\langle \Psi_f^-(\mathbf{r}_1,\mathbf{r}_2,\mathbf{r}_3)\left|\frac{Z}{r_1}-\frac{1}{r_{12}}-\frac{1}{r_{13}}\right|\psi_i(\mathbf{r}_1,\mathbf{r}_2,\mathbf{r}_3)\right\rangle, \tag{11}$$

where ψ_i is given by Eq. (5) and

$$\Psi_f^- = \exp(\mathbf{ik}_f\cdot\mathbf{R})\exp(-\lambda_f|\mathbf{r}_1-\mathbf{r}_2|)(2\pi)^{-3/2}M_3 \times\exp(\mathbf{ik_3}\cdot\mathbf{r_3})\ {}_1F_1(i\alpha_3,1;-i(k_3r_3+\mathbf{k}_3\cdot\mathbf{r}_3)) \tag{12}$$

with $\alpha_3=-Z/k_3$, $R=(\mathbf{r}_1+\mathbf{r}_2)/2$, and $M_3=\exp(\pi\alpha_3/2)\Gamma(1-i\alpha_3)$.

III. RESULTS AND DISCUSSIONS

We have computed the fully (triple) differential cross sections (TDCS) for the simultaneous transfer and ionization process in a positron-helium atom collision in which the

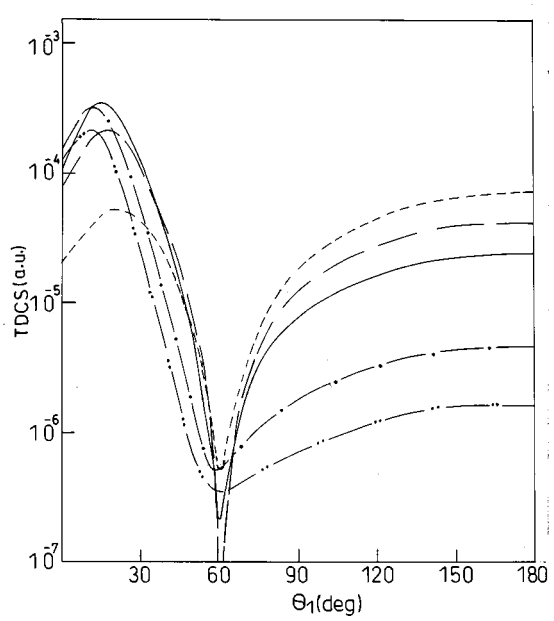

FIG. 1. Angular distribution of the Ps formation in the transfer ionization (TI) against the Ps scattering angle θ_1 in atomic units (a.u.) for different incident positron energies (E_i). Ejected electron energy $E_b=5$ eV, ejected angle $\theta_2=4°$, azimuthal angles are $\phi_1=0°$ and $\phi_2=180°$. Dashed curve, $E_i=125$ eV; long-dashed curve, $E_i=150$ eV; solid curve, $E_i=175$ eV; long-dashed–dot curve, $E_i=250$ eV; and long-dashed–double-dot curve, $E_i=300$ eV.

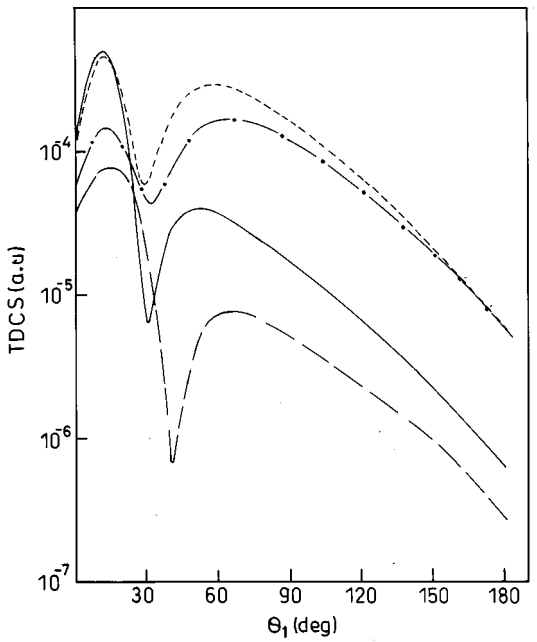

FIG. 2. Same angular distribution as in Fig. 1 for the fixed ejection angle $\theta_2=90°$ with two different incident e^+ energies (E_i) and two different ejected energies (E_b). Dashed curve, $E_i=150$ eV and $E_b=5$ eV; long-dashed–dot curve, $E_i=150$ eV and $E_b=25.93$ eV; solid curve, $E_i=250$ eV and $E_0=5$ eV; and long-dashed curve, $E_i=250$ eV and $E_b=59.27$ eV.

transferred electron forms a Ps atom in its ground state with the incident positron while the other electron is ionized in a single collision. Both the dynamics of the Ps atom and the ejected electron have been studied. The corresponding Born cross sections have also been studied by setting α_2 and α_{23} equal to zero in Eq. (8). In the present work the incident energy of the positron varies from the threshold energy to ~500 eV. The threshold energy for transfer is determined by the ionization energies of He and Ps and is given by $E_{\rm th}(T)=E_{\rm ion}({\rm He}(1s))-E_{\rm ion}({\rm Ps}(1s))=24.59-6.8=17.79$ eV, while the threshold energy for the transfer ionization (TI) is given by $E_{\rm th}({\rm TI})=17.79+54.4=72.19$ eV, since the second ionization energy of He is 54.4 eV.

Figure 1 displays the angular distribution of Ps formation following the transfer-ionization process against the Ps scattering angle θ_1 for different incident energies ($E_i=125-300$ eV) while the ejected electron energy (E_b) and the ejected angle are kept fixed at $E_b=5$ eV and $\theta_2=4°$, respectively. The azimuthal angles are fixed at $\phi_1=0°$ and $\phi_2=180°$. As is evident from Fig. 1, all the Ps distribution curves show a forward peak at around 10°–20° and a dip around 58°–62°, depending on the incident energy. In the TI process the excess energy is shared by the two outgoing particles, the ionized electron and the Ps in unknown proportions. Since the higher incident energy (E_i) for a fixed ejected energy (E_b) corresponds to a higher value of Ps energy, it appears from Fig. 1 that the higher the Ps energy, its distribution is more and more favored in the forward direction, i.e., the peak occurs at a lower angle (θ_1) with increasing incident energy. In contrast, in the backward direction the distribution is higher for lower Ps energy. This angular behavior of the Ps distribution is quite physical as was also noted in a pure transfer process [16].

In Fig. 2 we have demonstrated another Ps angular distribution in the TI process at an ejection angle $\theta_2=90°$ for two incident energies ($E_i=150$ eV and $E_i=250$ eV) and two different ejected energies (a) for $E_b=5$ eV and (b) for equal velocity of the two outgoing particles (e.g., the Ps and the ejected electron) with ϕ_1, ϕ_2 the same as in Fig. 1. Figure 2 reveals one interesting feature in all the curves, i.e., the occurrence of a double peak, one at a very small angle (~10°–15°) and the other at around (~50°–65°), depending on the incident as well as ejection energies. Further, regarding the position of the peaks, it may be noted that with increasing incident energy (E_i) (with fixed E_b) the peak positions shift towards a lower scattering angle (θ_1). In contrast, with increasing ejection energy E_b (for fixed E_i) the positions of the peaks shift towards a larger angle.

Figure 3 displays similar Ps distribution as in Fig. 2 but for two other ejection angles $\theta_2=45°$ and $\theta_2=180°$ while keeping E_b fixed at 5 eV. The double-peak structure has been noted for these two ejection angles also. However, for $\theta_2=180°$, the qualitative nature of the curves are somewhat different from that for $\theta_2=90°$ or 45° (see Figs. 2 and 3). In the former case ($\theta_2=180°$); instead of two distinct peaks (obtained for $\theta_2=90°$ and 45°), the curve starts from a maximum at zero angle and then, following a minima, a distinct peak occurs at around (~33°–35°). The depth of the minima becomes more and more sharp with increasing incident energy. From Figs. 1, 2, and 3 it may further be inferred that

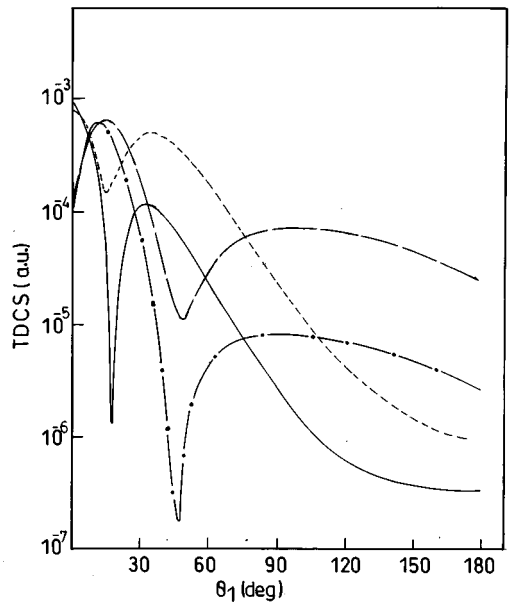

FIG. 3. Same as Fig. 2 with two different ejection angles and the ejected energy fixed at $E_b=5$ eV. Solid curve, $E_i=250$ eV and $\theta_2=180°$; long-dashed–dot curve, $E_i=250$ eV and $\theta_2=45°$; dashed curve, $E_i=150$ eV and $\theta_2=180°$; long-dashed curve for $E_i=150$ eV and $\theta_2=45°$.

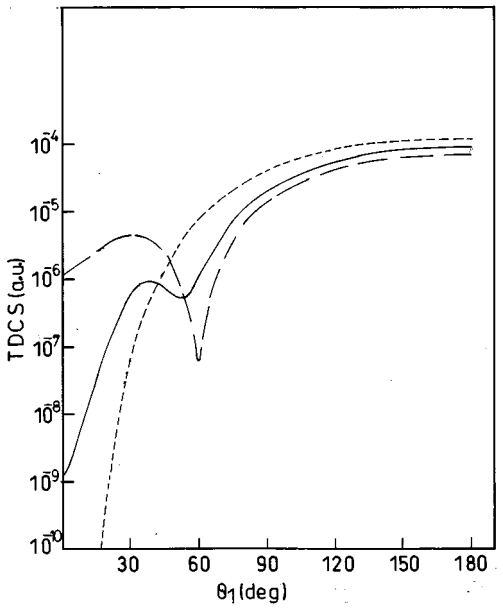

FIG. 4. Same angular distribution as in Fig. 1 for the fixed positron energy $E_i=100$ eV with different ejected electron energies (E_b). Long-dashed curve, $E_b=3$ eV; solid curve, $E_b=5$ eV; and dashed curve, $E_b=10$ eV.

when the ionized electron is ejected in the forward direction (e.g., $\theta_2=4°$, Fig. 1) the scattering of Ps in the backward angles is quite significant as compared to that in the forward direction. In contrast, for the backward or perpendicular ejection of the ionized electron (e.g., $\theta_2=180°$ in Fig. 3 and 90° in Fig. 2) the Ps distribution is almost negligible as compared to the corresponding forward angular distributions.

The double-peak structures (or shoulder-type structures) occurring in the Ps distribution (in Figs. 2 and 3) may be attributed to the Thomas double-scattering [17] mechanism predicted for charge transfer or transfer ionization [7,9] problems in the case of heavy-particle projectiles in high-energy regime. The simultaneous capture and ionization process (TI) may proceed mainly via two mechanisms. Either it can occur due to two independent interactions (uncorrelated) between the positron and two target electrons in separate encounters or it may arise due to the correlated e^+-e-e scattering (two successive binary collisions) in which the e^+ first scatters inelastically at one of the target electrons and then in a second interaction this electron scatters at the other target electron (through the electron-electron correlation), so that finally one target electron is emitted into the target continuum while the other electron forms a bound state with the incident e^+ to form a Ps atom. For heavy-particle impact also, such correlated projectile-electron-electron scattering mechanism leading to TI is responsible for the narrow peak (at a critical angle $\sim$0.3 mrad) observed [9] in the angular (scattering angle) dependence of the He^{++} fraction from single-electron capture reactions in $H^+ + He$ collision at high incident energies ($\sim$200–500 keV).

The signature of the Thomas peak was also observed [7] in the absolute energy and angular differential cross sections for electron emission at high incident energies in the same TI process and the peak was similarly attributed [7] to the correlated H^+-e-e scattering mechanism.

However, for a light projectile (as in the present case), the so-called Thomas peak [17] occurs at a comparatively much lower incident energy (e.g., 150 eV in the present case). Of course this feature becomes increasingly marked as the incident energy increases. This is also corroborated by the experimental findings where the differential TI cross sections have been measured for the ionization of argon atoms by a positron impact [10]. In their measurements [10] also, the signature of the double peak was noted at a much lower incident e^+ energy. Comparing Figs. 1, 2, and 3, it may be noted, however, that the double-peak structure is absent for low ejection angles (e.g., 4° in Fig. 1).

In Fig. 4 we have plotted the Ps distribution against the scattering angle θ_1 for a low incident energy ($E_i=100$ eV) and for three different ejected energies ($E_b=3$, 5, and 10 eV) while keeping the other parameters the same as in Fig. 1. Similar behavior (as described above for Fig. 1) is also reflected in Fig. 4, i.e., the Ps distribution for higher ejected energy which in turn corresponds to lower Ps energy is favored in the backward direction. The curves for lower E_b (e.g., $E_b=3,5$ eV) in Fig. 4 show a small peak at around $\sim$30°–40° scattering angle while for higher E_b ($E_b=10$ eV) the distribution increases steadily with increasing scattering angle. Figure 4 indicates that at $E_i=100$ eV, the Ps is scattered preferentially in the backward direction for all the ejected energies. This feature becomes increasingly marked as the ejected energy E_b increases. This is probably because at $E_i=100$ eV and for the E_b chosen in Fig. 4, the available energy to Ps is very low ($\sim$17.8–24.8 eV) and according to the previous discussions (for Fig. 1) the back-

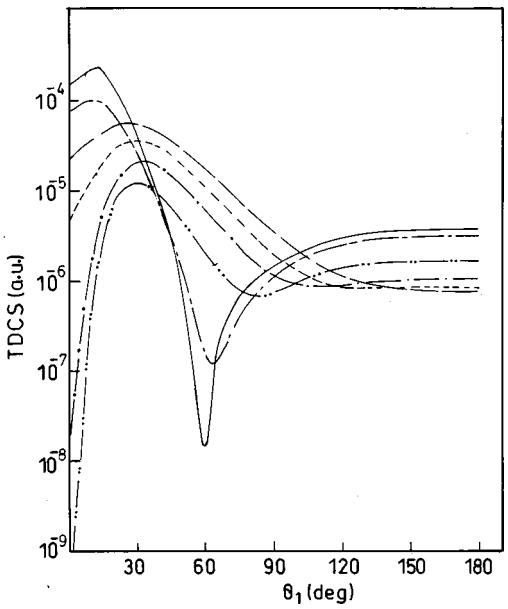

FIG. 5. Same as Fig. 4 with incident energy fixed at $E_i = 250$ eV and the solid curve for $E_b = 10$ eV; long-dashed–short-dashed curve, $E_b = 20$ eV; long-dashed–double-dot curve, $E_b = 50$ eV; long-dashed–dot curve, $E_b = 75$ eV; dashed curve, $E_b = 88.9$ eV; long-dashed curve, $E_b = 100$ eV.

ward contribution dominates over the forward one at this low value of Ps energy.

Figure 5 displays similar Ps angular distribution for a higher incident energy ($E_i = 250$ eV) and for different ejected energies ($E_b = 10-100$ eV) with fixed ejection angle $\theta_2 = 4°$. Here also the lower E_b (i.e., higher Ps) curves are highly peaked in the forward direction than those for higher E_b. Unlike Fig. 4 (for $E_i = 100$ eV), in Fig. 5, the Ps distribution is significantly higher at forward angles than at extreme backward (180°). This behavior again corroborates the fact that since for higher E_i (250eV) and for the E_b's shown in Fig. 5, the Ps scatters with higher energy (as compared to Fig. 4), the distribution is more favored at small angles.

Figure 6 displays the corresponding first Born results [see Eq. (11)] for the angular distribution of Ps formation for different incident e^+ energy ($E_i = 150-300$ eV) while keeping other parameters fixed (as in Fig. 1). As is noted from the figure, the first Born curve shows no significant structure, instead it falls off almost monotonically with the scattering angle θ_1 except for a very small angle ($\theta_1 \sim 10°$). The first Born approximation (FBA) cross section decreases with increasing incident energy as is expected physically. Since the TI process involves a simultaneous two-electron transition in which the electron-electron correlation plays the most dominant role, the first Born approximation which neglects the higher-order effects altogether is not supposed to be valid for such a process even at high incident energy.

To describe the ejection angular distribution (Figs. 7–10) we have adopted the conventional notation for a pure ionization process, i.e., the so-called binary region (in a pure ionization process) is represented by the 0°–180° region ($\phi_2 = 180°$) while the portion 0° to −180° ($\phi_2 = 0°$) represents the so-called recoil region.

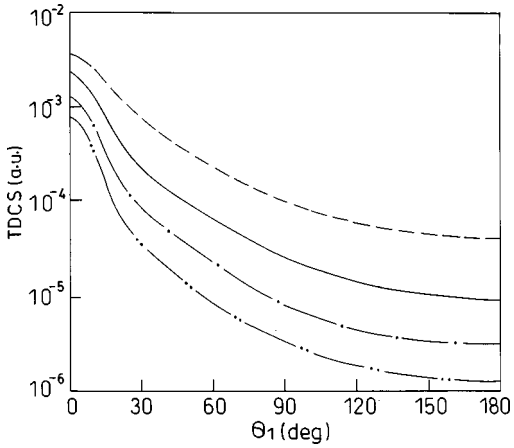

FIG. 6. Same as Fig. 1 but for the first Born approximation [Eq. (11)]. Long-dashed curve, $E_i = 150$ eV; solid curve, $E_i = 200$ eV; long-dashed–dot curve for $E_i = 250$ eV; and long-dashed–double-dot curve, $E_i = 300$ eV.

Figure 7 exhibits the angular distribution of the ejected electron for different incident energies but for the fixed ejected energy ($E_b = 5$ eV) and the fixed scattering angle of Ps ($\theta_1 = 4°$). Unlike the angular distribution of the ejected electron in a single-ionization process (where two distinct lobes appear), here in the TI process the ejection angular distribution curve (except for the curve at $E_i = 125$ eV) shows a broad hump in the binary region while in the recoil region no such structure is obtained. It should be pointed out here that in the present model, the ionization of the second target electron is mainly caused by the electron-electron correlation effect instead of the projectile-electron interaction as in the case of pure ionization. However, the maximum value of the cross section occurs at the extreme backward angles ($\theta_2 = \pm 180°$) both in the binary and the recoil regions. Some exception occurs at $E_i = 125$ eV (in Fig. 7), where the

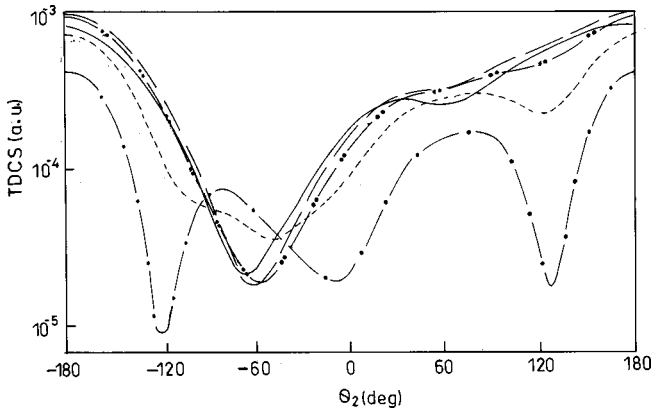

FIG. 7. Angular distribution of the ejected electron in the TI against ejection angle θ_2 in atomic units (a.u.) for different incident positron energies (E_i). The Ps scattering angle is fixed at $\theta_1 = 4°$ and the ejected electron energy is fixed at $E_b = 5$ eV. Azimuthal angles $\phi_1 = 0°$ and $\phi_2 = 0°$ and 180°. Long-dashed–dot curve, $E_i = 125$ eV; dashed curve, $E_i = 150$ eV; long-dashed–double–dot curve, $E_i = 175$ eV; long-dashed curve, $E_i = 200$ eV; and solid curve, $E_i = 250$ eV.

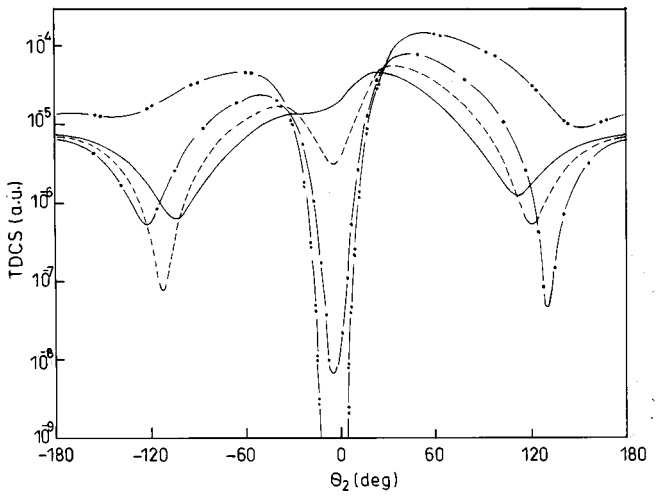

FIG. 8. Same angular distribution as in Fig. 7 with different ejected energies and a fixed incident positron energy $E_i = 250$ eV. Long-dashed–double-dot curve, $E_b = 50$ eV; long-dashed–dot curve, $E_b = 75$ eV; dashed curve, $E_b = 88.9$ eV; and solid curve, $E_b = 100$ eV.

curve shows two distinct lobes in the binary and recoil region (as in the case of pure ionization), although as in the other cases (in Fig. 7) the magnitude in the two region (binary and recoil) is maximum at $\theta_2 = \pm 180°$.

It is well known that the charge-transfer process is dominant at low incident energy and for the positron-helium atom system the Ps formation cross section was found [16] to be significant only up to the incident positron energy ~150 eV, after which the contribution decreases very rapidly. On the other hand, the pure ionization process is more important at higher incident energies as compared to the Ps formation process. Figure 7 corroborates this fact since, as may be noted from the figure, the magnitude of the ejected angular

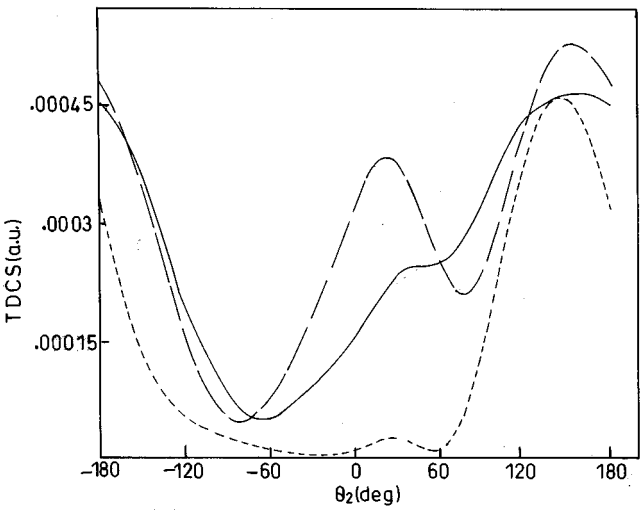

FIG. 9. Same angular distribution as in Fig. 7 with two different incident energies and two different scattering angles. The ejected energy is fixed at $E_b = 10$ eV. Solid curve, $E_i = 250$ eV and $\theta_1 = 4°$; dashed curve, $E_i = 250$ eV and $\theta_1 = 45°$; long-dashed curve, $E_i = 500$ eV and $\theta_1 = 4°$ (results are multiplied by a factor of 10).

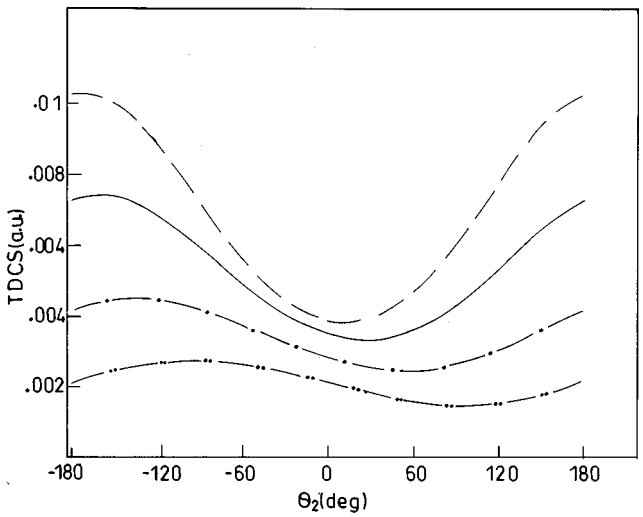

FIG. 10. Same as Fig. 7 but for the first Born approximation [Eq. (11)]. Long-dashed curve, $E_i = 125$ eV; solid curve, $E_i = 150$ eV; long-dashed–dot curve, $E_i = 175$ eV; and long-dashed–double-dot curve, $E_i = 200$ eV.

distribution mainly governed by the maximum values of the curve enhances as the incident energy increases up to $E_i = 200$ eV (in Fig. 7) while at $E_i = 250$ eV the cross section starts decreasing. However, the apparent anomalous behavior of the $E_i = 250$ eV curve in Fig. 7 may probably be attributed to the following fact. The incident energy $E_i = 250$ eV (in Fig. 7) for the TI process is sufficiently high for which the contribution of the Ps formation cross section becomes negligible [16] and even for the ionization reaction which then mainly controls the TI process, this energy is still high so that the corresponding result (in Fig. 7) lies below the results of 175 eV. This behavior occurs in view of the fact that for a fixed ejected energy (E_b), the probability for the single-ionization process in an e^+-He atom system decreases with the increase of incident e^+ energy [18] in the high-energy regime.

Figure 8 represents the angular distribution for the ejected electron (θ_2) for some higher values of ejected energies ($E_b = 50$–100 eV) while keeping the incident e^+ energy ($E_i = 250$ eV), θ_1 and ϕ_1 fixed. As is evident from Fig. 8, the magnitude of both the binary and recoil peaks decreases with increasing ejected energy, as is expected physically. This feature is also well established in pure single-ionization processes [19]. Further, regarding the position of the peaks it may be noted that the peak (both binary and recoil) positions shift towards smaller ejection angles as the ejected energy increases. Another interesting feature in TI which is absent in pure ionization is the occurrence of two minima (one is almost around 0° and the other at a higher angle) in the recoil region (in Fig. 8).

Figure 9 displays the same θ_2 distribution as in Fig. 8 but for a lower value of E_b (10 eV) with two different incident energies ($E_i = 250$ and 500 eV) and two different scattering angles ($\theta_1 = 4°$ and 45°). In view of the fact that the peak positions shift towards a larger angle (θ_2) for lower E_b, it may be inferred from Figs. 8 and 9 that as E_b decreases (say down from $E_b = 100$ eV to 10 eV) the recoil maximum shifts

exactly to 180° (see Fig. 9). Figure 9 (for lower $E_b = 10$ eV) reveals an important feature, a double-peak structure in the binary region which is absent for the higher ejection energy (see Fig. 8). It is also noted from Fig. 9 that the signature of the double peak is more and more marked with increasing incident energy. In fact we have also computed the θ_2 distribution for the same geometry but with another high value of incident energy, $E_i = 1000$ eV (not shown in the figure) and we have noted this behavior. Figure 9 also indicates that this double-peak structure has also been found for a larger scattering angle (e.g., $\theta_1 = 45°$). This double peak, as in the case of the Ps distribution, might again be assigned to the correlated $(e^+\text{-}e\text{-}e)$TI process [7,8].

Figure 10 depicts the first Born ejection angular differential cross sections in the TI process for different incident energies (125–200 eV) with fixed values of E_b, θ_1, and ϕ_1 (as in Fig. 7). As may be noted from the figure, the first Born approximation (FBA) which neglects all higher-order interactions is unable to exhibit any structure as in the case of the FBA Ps distribution (Fig. 6). Instead, in the FBA the angular distribution curve for the ejected electron (Fig. 10) rises almost steadily from the forward direction (0°) to the backward direction (180°) in the binary region. In the recoil region, however, the peak value occurs at a slightly lower angle (~95°–170°) than 180° (unlike the binary region), depending on the incident energy. The position of the recoil peak shifts towards a lower angle with increasing incident energy. All the FBA curves in Fig. 10, however, maintain uniformly the usual physical feature that the cross section decreases with increasing incident e^+ energy.

In Fig. 11 we have plotted the fully differential cross section (TDCS) as a function of the ejected energy E_b for a particular dynamics, e.g., by choosing the angle of ejection (θ_2) to be identical with the scattering angle (θ_1) of the Ps and the angle is kept fixed at 45°. The corresponding azimuthal angles are chosen as $\phi_1 = 0°$ and $\phi_2 = 180°$ while the incident energy is kept fixed at $E_i = 200$ eV. The curve is almost symmetric in nature and exhibits a single peak at around $E_b \approx 60$ eV and then falls down to $E_{bc} = 127.8$ eV. In fact this value of E_b gives a cutoff (E_{bc}) for this TI process since at this particular E_i (200 eV), the energy of the scattered Ps [200–127.8−threshold energy for TI (72.19)≈0] becomes zero. Obviously the value of E_{bc} varies with incident energy E_i as guided by the energy conservation relation [see Eq. (9)]. In a similar manner, the same cutoff value can be found (for a particular E_i) in the triple differential cross-section curve as a function of the Ps energy for which the ejected energy E_b goes to zero.

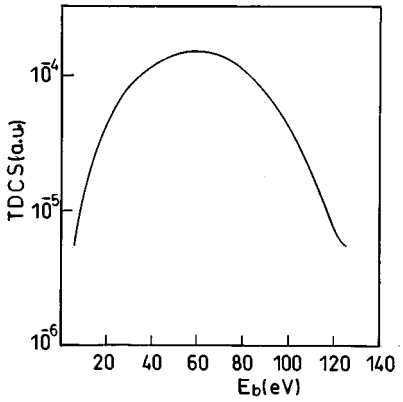

FIG. 11. Fully differential cross sections (TDCS) following the TI process against ejected energy (E_b). The Ps scattering angle and the angle of ejection both are fixed at $\theta_1 = \theta_2 = 45°$, azimuthal angles are fixed at $\phi_1 = 0°$ and $\phi_2 = 180°$, and the incident positron energy is fixed at $E_i = 200$ eV.

IV. CONCLUSION

The present work deals with a two-electron transition process in an e^+-He atom system where two competing processes occur simultaneously, e.g., the formation of Ps and the ejection of another electron. The present model takes proper account of the correlation effect in both the channels, and hence is expected to give a reasonable result for the fully differential TI cross sections. For the light projectile (e^+), so far as our knowledge goes, there is no other theoretical result for the TI process in the fully differential level and as such the present detailed results (both the Ps and ejection distributions) are supposed to give some guidelines for future experimentalists.

As far our knowledge goes, the measurements [10–12] available so far in the literature for the TI process by positron impact are for some noble-gas systems. Further, all the experimental data [10–12] refer to either total-ionization cross sections [11,12] or to the single differential cross sections [10], i.e., the measurements have not been performed in the fully differential level which is the subject of the present study. We are thus not in a position to compare the present results (quantitatively) in any way with the measurements. Qualitatively, it may be mentioned that the present study more or less corroborates the experimental findings [11,12] that in the double ionization (DI), the Ps channel is strongly suppressed in the second ore gap region for some noble gases (e.g., He and Ne) where TI is the only open channel for the DI process of the target atom. In the present model also, we have noted that the present TI differential cross sections are almost negligible in the second ore gap region (~72.2–80 eV) at $E_i = 78$ eV (not shown in the figure).

[1] J. H. McGuire, Phys. Rev. A **36**, 1114 (1987).
[2] J. F. Reading and A. L. Ford, J. Phys. B **20**, 3747 (1987).
[3] J. H. McGuire, Adv. At., Mol., Opt. Phys. **29**, 217 (1991).
[4] F. Martin and A. Salin, Phys. Rev. Lett. **76**, 1437 (1996).
[5] J. F. Reading, T. Bronk, and A. L. Ford, J. Phys. B **29**, 6075 (1996).
[6] F. Martin and A. Salin, Phys. Rev. A **54**, 3990 (1996).
[7] J. Palinkas, R. Schuch, H. Cederquist, and O. Gustafsson, Phys. Scr. **42**, 175 (1990).
[8] J. Palinkas, R. Schuch, H. Cederquist, and O. Gustafsson,

Phys. Rev. Lett. **63**, 2464 (1989).
[9] E. Horsdal, B. Jensen, and K. O. Nielsen, Phys. Rev. Lett. **57**, 1414 (1986).
[10] T. Falke, W. Raith, and M. Weber, Phys. Rev. Lett. **75**, 3418 (1995).
[11] H. Bluhme, H. Kundsen, J. P. Merrison, and M. R. Poulsen, Phys. Rev. Lett. **81**, 73 (1998).
[12] J. Moxom, D. M. Schrader, G. Laricchia, Jun Xu, and L. D. Hulett, Phys. Rev. A **60**, 2940 (1999).
[13] R. A. Bonham and D. A. Kohl, J. Chem. Phys. **45**, 2471 (1966).
[14] R. Biswas and C. Sinha, J. Phys. B **28**, 1311 (1995).
[15] R. Biswas and C. Sinha, Phys. Rev. A **54**, 2944 (1996).
[16] B. Nath and C. Sinha, Eur. Phys. J. D **6**, 295 (1999).
[17] L. H. Thomas, Proc. R. Soc. London, Ser. A **114**, 561 (1927).
[18] R. Biswas and C. Sinha, Phys. Lett. A **194**, 197 (1994).
[19] M. Brauner, J. S. Briggs, and H. Klar, J. Phys. B **22**, 2265 (1989).